Power Engineering and Engineering Thermophysics
https://www.acadlore.com/journals/PEET

Optimization of Shell and Tube Condenser Effectiveness via PSO Algorithm Coupled with Forced Convection Characterization in Multiphase Systems

Nu Rhahida Arini[1*], Allisa Dwi Putri[1], Wahyu Nur Fadilah[1], Abir Hasnaoui[2]

[1] Department of Mechanical and Energy Engineering, Politeknik Elektronika Negeri Surabaya, 60111 Surabaya, Indonesia
[2] Department of Electrical Engineering, University of Sciences and Technology of Oran-MB.Oran, 31000 Bir El Djir, Algeria

* Correspondence: Nu Rhahida Arini (Arini@pens.ac.id)

Received: 08-29-2023 **Revised:** 09-22-2023 **Accepted:** 09-30-2023

Citation: N. R. Arini, A. D. Putri, W. N. Fadilah, and A. Hasnaoui, "Optimization of shell and tube condenser effectiveness via PSO algorithm coupled with forced convection characterization in multiphase systems," *Power Eng. Eng. Thermophys.*, vol. 2, no. 4, pp. 188–198, 2023. https://doi.org/10.56578/peet020401.

Abstract: In the design of shell and tube heat exchangers encompassing a condensing zone, meticulous attention is required due to the complexities surrounding forced convection in multiphase systems. Despite extensive research, the intricacies within these multiphase systems have remained elusive, rendering the heat transfer coefficient unresolved. In this study, a novel methodology is introduced to elucidate the thermal characteristics of forced convection within the condensing region of shell and tube condensers. An amalgamation of theoretical methods, specifically the Logarithmic Mean Temperature Difference (LMTD), and empirical data sourced from industrial operations forms the foundation of this approach. Upon rigorous analysis employing both Power Law Analysis and Logarithmic Linear Regression, a correlation in terms of $N_u = C \cdot Re^m \cdot Pr^n$ within the condensing region was discerned using Buckingham Pi Theorem. Findings revealed coefficients of C=1.15, m=0.893, and n=13.442. For optimization purposes, the Particle Swarm Optimization (PSO) Algorithm was employed. A focused examination of parameters such as tube length, tube outside diameter, baffle spacing, shell diameter, number of tube passings, and tube wall thickness revealed that by attenuating their values by 30%, 46%, 80.3%, 8%, 50%, and 61.9% respectively, a substantial increase in condenser effectiveness was observed, elevating the value from 0.9473 to 4.299.

Keywords: Condenser effectiveness; Condensing zone; Forced convection; Particle Swarm Optimization (PSO) algorithm

1 Introduction

Heat exchange through forced convection, a mechanism driven by devices such as pumps and compressors, has been established as a critical process across various industrial applications [1–3]. Within this realm, heat exchangers play an instrumental role, with the shell and tube variety emerging as the most prevalent. However, while theoretical methods including LMTD and Number of Transfer Units (NTU) have been reviewed and applied for designing such exchangers [4], challenges arise when forced convection interfaces with multiphase fluids. The intricate nature of multiphase processes has, thus far, obfuscated precise definitions of the heat transfer coefficient. A notable instance of this complexity is manifested in the condensing regions of shell and tube condensers, employed across industries ranging from batteries to nuclear power plants. Consequently, there remains a pressing need to articulate a method that effectively characterizes forced convection, especially within condensing regions.

The design intricacies of multiphase shell and tube heat exchangers, pivotal in industrial settings, necessitate meticulous attention to attributes such as working fluid temperature, heat flow rate, and condenser geometry. The inherent complexity of multiphase flows stems from the concurrent presence of disparate phases, each bearing unique mechanical and chemical attributes. This multifaceted nature is further amplified by the diverse parameters impacting both efficiency and the overarching economic viability of industrial operations.

The Lattice Boltzmann Methods, for instance, have been employed to decipher multiphase flows, as highlighted in studies like that of study [5]. Such methods, adaptable to both theoretical and numerical scenarios, offer promise.

Notably, a two-pronged approach, blending both numerical and experimental methodologies, has been underscored for its precision in several works [6–10].

Amid the array of potential optimizations, a consistent focus has been the pursuit of heightened effectiveness within shell and tube condensers. Empirical evidence from research [11–14] suggests the viability of parameter optimization as a conduit for bolstered production at reduced costs. Within this optimization landscape, the PSO algorithm has garnered attention [10, 15–17]. Defined as a technique that iteratively refines solutions (or particles) against a quality benchmark, the PSO algorithm modulates particle movement within the problem space predicated on specified functions governing particle position and velocity [15]. Its merits lie in its simplicity, efficiency, and ease of implementation relative to other numerical methodologies.

At its core, the condensing zone within a shell and tube condenser represents a pivotal region. Situated within the shell component, this zone witnesses the heat medium transitioning from vapor to its condensed form, thereby transferring heat to the cooling medium within the tube. This interaction propels forced convection, leading the cooler fluid in the tubes to heat and vaporize. The resultant vapor, post-condensation, reverts to condensate water, which, in turn, can be repurposed for varied industrial processes [18]. Given the centrality of this process, the ability to precisely design and predict heat transfer characteristics within the condensing zone is of paramount importance.

This study aims to present a method that not only characterizes multiphase forced convective heat transfer but also leverages the PSO algorithm to optimize heat exchanger effectiveness within the condensing zone of shell and tube condensers. The overarching intent is to streamline the calculation of general thermal performance within the condensing zone of such condensers.

2 Methodology

The present study is divided into two primary objectives. Firstly, the heat transfer characteristic within the condensing zone of the shell and tube condenser is elucidated. Secondly, an optimization of the condenser effectiveness is pursued.

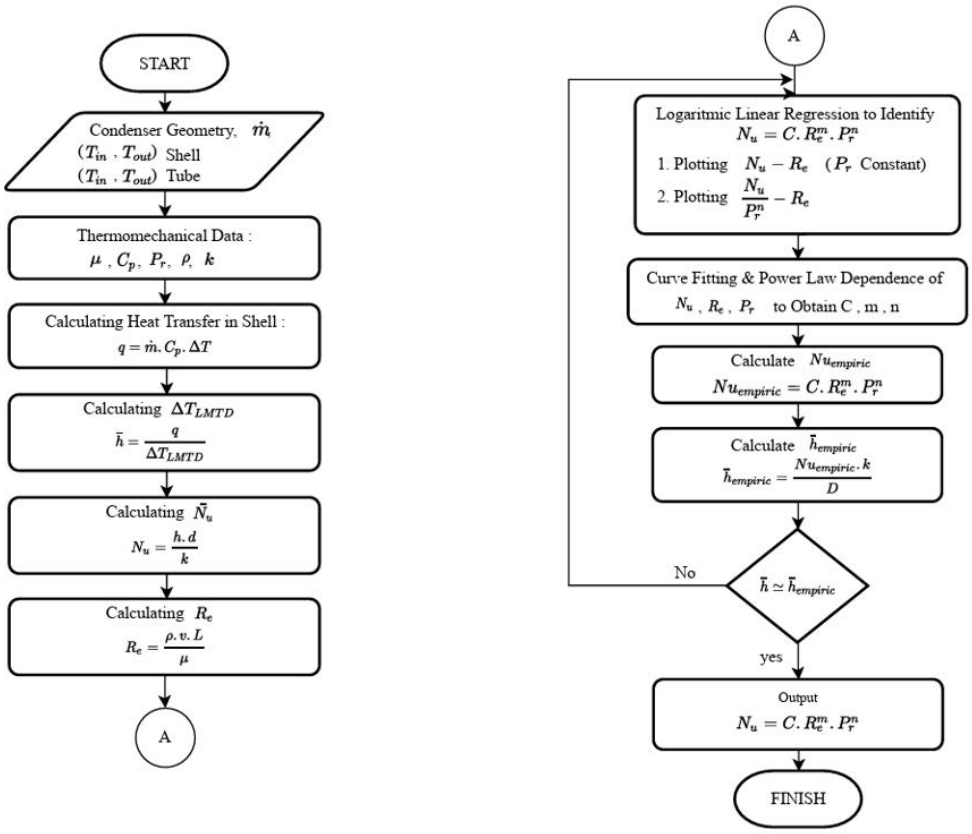

Figure 1. Flowchart delineating design and formulation of the condensing region within the condenser

In the preliminary segment, a proposed technique for discerning the heat transfer characteristic is illustrated in Figure 1. Utilizing a blend of empirical and theoretical data, the heat transfer characteristic was analyzed. Data for this analysis was extracted from operational records of a shell and tube condenser in an industrial setting spanning three months. It was observed that saturated steam, in the condensing zone, flowed within the shell and was subsequently

condensed by water flowing through the tube banks. The condensed medium was identified to be pure vapor, leading to an assumption that heat transfer occurs at the saturation temperature within the shell [19, 20]. For the purposes of this study, no heat dissipation was assumed.

Even though saturated steam, a two-phase fluid, is prevalently utilized as a heating medium in industrial processes, complexities inherent in multiphase phenomena render the heat transfer characteristic somewhat elusive. The current research introduces an advanced and straightforward technique to determine the forced convective heat transfer characteristic within the condensing zone of shell and tube condensers. This characteristic is represented by an average convection heat transfer coefficient, symbolized as $\bar{h}$. This coefficient, covering the entirety of the part under study, is denoted as the average heat transfer coefficient ($\bar{h}$). From the average Nusselt Number (N_u), this coefficient can also be derived. This derivation involves a correlation that incorporates N_u, Re, and Pr. In a theoretical context, $\bar{h}$ is deduced from heat transfer within the tubes when specific surface areas are engaged. Under conditions where the water within the tube is heated from an inlet temperature T_{in} cooling water to an outlet temperature T_{out} cooling water, and where pressure remains constant with no heat loss, $\bar{h}$ is formulated using Eq. (1):

$$\bar{h} = \frac{4}{A_s \cdot \Delta T_{LMTD}} \tag{1}$$

where, ΔT_{LMTD} is articulated as:

$$\Delta T_{LMTD} = \frac{\Delta T_A - \Delta T_B}{\ln\left(\frac{\Delta T_A}{\Delta T_B}\right)} \tag{2}$$

where, ΔT_A and ΔT_B represent the differences between the shell's inlet temperature and tube's outlet temperature, and the shell's outlet temperature and tube's inlet temperature, respectively. Furthermore, the average conductive coefficient is computed to deduce N_u using Eq. (3):

$$N_u = \frac{hD}{k} \tag{3}$$

For the empirical approach, a correlation was established between the dependent N_u and both Re and Pr. Initially assessed through the Buckingham Pi Theorem (20), this theorem encompasses all parameters inherent in the heat transfer formula, both dependent and independent. For the shell and tube heat exchanger, the theorem designates empirical dimensional parameters that may influence the heat exchanger's behavior, such as flow velocity, density, thermal conductivity, specific heat capacity, dynamic viscosity, water convection heat transfer coefficient, and tube diameter. These seven-dimensional parameters were subsequently grouped to yield dimensionless numbers.

By processing the grouped parameters, dimensionless parameters Re and Pr were derived from the mechanical properties of the fluid in light of its film temperature. Data from industrial operations, such as inlet and outlet temperatures of water, inlet and outlet temperatures of steam, and mass flow rates of both water and steam, informed this temperature. Through mathematical methodologies (elaborated in Section 2.2), constants pertaining to the heat transfer coefficient, in terms of powers of Re (m) and Pr (n) and C, were acquired to shape Eq. (4):

$$N_u = C \cdot Re^m \cdot Pr^n \tag{4}$$

Folling this, $N_{u_{\text{empiric}}}$ was discerned using the resolved empirical formula of Eq. (4). The next phase entailed the computation of h_{empiric} using Eq. (3). The convective coefficients, both theoretical and empirical, were subsequently juxtaposed to validate the results.

2.1 Parameters of Convective Heat Transfer

The convective heat transfer coefficient, representing the heat transfer between the fluid in the shell and the fluid in the tube within the condensing zone of a condenser, was extensively analyzed. For this examination, both empirical and theoretical evaluations were harmoniously integrated. Empirical data was sourced from an industrial case study, where water functioned as the working fluid on both the shell and tube sides. Such a dual-method approach, combining empirical and theoretical analyses, mirrors the methodological foundations explored by Gunes [21]. In his research, forced convection heat transfer characteristics in water flowing inside and outside a laboratory-scaled double pipe heat exchanger tube were investigated. With the employment of a pump, water was introduced into the heat exchanger, leading to the manifestation of forced convection heat transfer.

In the empirical approach adopted here, mechanical properties data was derived using film temperature. This temperature was calculated based on the inlet and outlet temperatures of both steam and water. A consistent temperature was maintained by the steam within the tubes throughout the process. The surface temperature of these tubes was assumed to mirror the temperature of the water circulating within them. An assumption was made that conduction was absent in the system, due to the tube walls being perceived as exceptionally thin. Furthermore, the tube surface temperature was posited to be an average of the temperatures at the inlet and outlet sections. Consequently, Re and Pr were defined based on film temperature, which was predicated on the consistent steam temperature and the average water temperature.

Highlighting the correlation of dimensionless numbers is pivotal in comprehending the forced convection heat transfer characteristic. This analytical pathway has been previously treaded upon by Park [22]. His research emphasized forced convection in crossflow involving thin circular isothermal fins within tubes. Dimensionless parameters, Re and Pr, which were functions of N_u, were extracted from simulation outcomes generated by the Ansys FLUENT software. Mathematical methods, such as curve-fitting procedures, were subsequently applied to procure correlations of dimensionless numbers for both circular fins and tube walls. Through the application of Logarithmic Linear Regression Analysis, a distinct correlation of dimensionless numbers, encapsulating the characteristics of forced convection heat transfer on a sphere, was deduced. Such methodology was emulated in the present study, focusing on the characteristics of forced convection within the condensing zone of an industrial condenser.

2.2 Mathematical Procedures for Analyzing Convective Heat Transfer Characteristics

In this research, a methodological approach was undertaken to deduce heat transfer characteristics, specifically expressing N_u as a function of Re and Pr. The Buckingham Pi Theorem, a renowned method for dimensional analysis, was employed to derive the heat transfer formula. Recognized for its capacity to streamline the complexity of experimental variables, the Buckingham Pi Theorem succinctly aggregates these variables into dimensionless parameters [10]. By leveraging this theorem, parameters influential to forced convection heat transfer, encompassing h, k, Cp, ρ, μ, v, and D, are consolidated into three primary dimensionless numbers: Re, Pr, and N_u. Such a grouping simplifies the correlation discovery process among these parameters, as elaborated in Eq. (4) [9].

Subsequent to this formulation, an assessment was conducted by plotting the three aforementioned dimensionless numbers on a unified graph. Similar procedures were reported in previous studies [23–25]. The analysis incorporates Logarithmic Linear Regression, Curve Fitting [26], and Power Law Analysis. Notably, Melissari and Argyropoulos [27] utilized Logarithmic Linear Regression to determine heat transfer characteristics. In their investigation, a correlation of dimensionless numbers, consisting of Re, Pr, and N_u, was formed. Experiments with liquid sodium and water flowing over spherical entities were executed. By plotting log N_u against log Re and log Pr individually, a correlation anchored on logarithmic linear regression was deduced, elucidating the relationship between N_u, Re, and Pr. Noteworthy parallels were observed between theoretical predictions and experimental findings.

Logarithmic linear regression, a transformative technique, converts a given function into a correlation with logarithmic values along both x and y axes. Originating from logarithmic transformation values, this method renders both independent and dependent variables in logarithmic forms. This transformation often becomes indispensable when non-linear relationships exist between dependent and independent variables. In such scenarios, the logarithmic form retains the linearity of the model while capturing the non-linear relationships.

In this analysis, Re and Pr were plotted, with each being a function of N_u. Once plotted using logarithmic regression analysis, the relationship of N_u to both Re and Pr was delineated. The correlation was structured to position the dependent variable in relation to an independent variable, holding other independent variables constant. With two independent variables present, two distinct correlations were visualized, each presenting N_u as the dependent variable. The initial plot, which treated N_u as a dependent variable against Re, yielded the function Re^m. The subsequent plot, which contrasted N_u with Pr, followed an analogous process and yielded the function Pr^n. When these dependent variables were plotted against a combination of independent variables, a constant (C) in the heat transfer characteristic formula emerged.

To conclude, the formula, denoting Re and Pr as dependent variables, was employed to ascertain the heat transfer characteristic N_u. In this phase, the estimated heat transfer characteristic was labeled N_u empiric. Concurrently, an empirical heat transfer coefficient, denoted $\bar{h}_{empiric}$, was discerned. The proximity of this value to its theoretical counterpart reaffirms the validity of the mathematical procedures employed.

2.3 Acquisition and Analysis of Industry-Derived Empirical Data

Empirical data assessed in this study were sourced from industrial operations of a shell and tube condenser. The specifications of this condenser are detailed in Table 1. Although various types of shell and tube condensers operate within the industry, it should be noted that the methodology proposed in this research is applicable to diverse shell and tube condenser configurations, not solely the one assessed here.

Table 1. Geometry of the condenser

Condenser Type	Surface Condenser
Shell diameter	9 ft
Tube outside diameter	19.05 mm
Tube length	6.500 mm
Tube thickness and material	1.2 mm, copper
Number of tubes	13112
Tube pitch	Triangle, 24 mm
Tube passes	4
Baffle spacing	6500 mm

Centrally situated within the condenser is a condensing zone, the depiction of which, inclusive of temperature distribution along the shell and tube sides, is provided in Figure 2. The working fluid, water, is observed to flow through both the shell and tubes. For the purpose of data collection, inlet and outlet temperatures from both zones, as well as the mass flow rate, were recorded, as presented in Table 2. Within the condenser, heat disperses and is subsequently transferred to the cooling water within the tubes. As water vapor enters the condensing zone's inlet on the shell side, it undergoes condensation, releasing heat. It is posited that no heat loss occurs during this process, implying all heat is transferred to the cooling water. The validity of this study will be ascertained by juxtaposing model-derived temperature results with actual industrial operational data.

Table 2. Operational parameters of the condenser

	May 01	May 02
Tin Steam $(^{\circ}\mathbf{C})$	290	287
Tout Seam $(^{\circ}\mathbf{C})$	41	41
Tin Cooling Water $(^{\circ}\mathbf{C})$	31	30
Tout Cooling Water $(^{\circ}\mathbf{C})$	38	37
Steam Flow Rate $(\mathbf{T/h})$	23.2	22.1
Cooling Waterflow Rate $(\mathbf{m^3/h})$	3310	3310

For clarity, "Tin steam" and "Tout steam" denote the temperatures of steam entering and exiting the shell, respectively. On the tube side, "Tin cooling water" and "Tout cooling water" represent the temperatures at which cooling water enters and exits all tubes. The flow rates of both steam and water are documented in the concluding columns of Table 2. The primary focus of this investigation pertains to the condenser's condensation zone, where heat transfer between water in the shell and tubes is observed. A consistent temperature distribution within the shell is maintained as steam condenses, as elucidated in Figure 2. Within this study's scope, it is the condensing zone alone that is examined, with an emphasis on the steam in the shell serving as the condensed fluid.

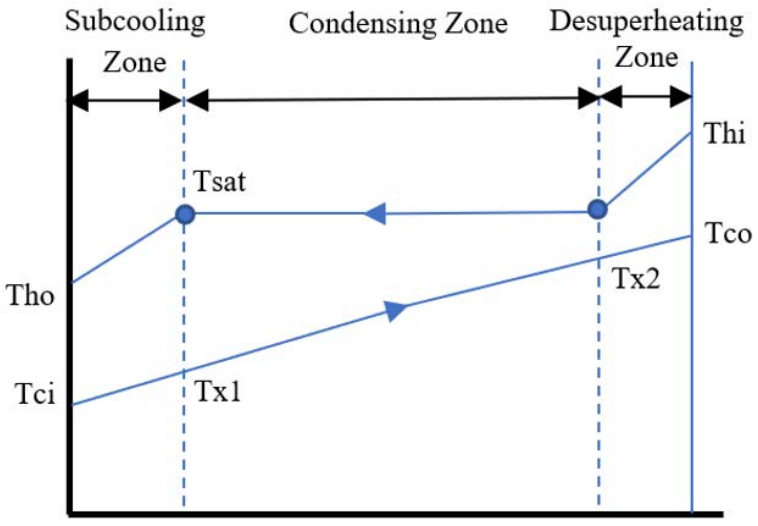

Figure 2. Illustration of the FEM via a flow chart

3 Application of PSO for Condenser Geometry

The PSO algorithm, designed for iterative problem-solving, utilizes a swarm of particles which traverse the problem space, adjusting positions based on the quality of solutions, as described by study [12]. Solutions, referred to as particles, are continually recalculated using specific functions associated with the position and velocity of said particles. The provisional best solution found thus far influences the movement of the particles. As a result, the collective set of particles, known as a swarm, ultimately converges upon the final best solution [12].

Within the PSO framework, agents, termed particles, traverse the search space in pursuit of the optimal solution. Each particle's trajectory is adjusted in accordance with both its own experience and the cumulative experience of the entire swarm. The three pivotal parameters for each particle include its current position, velocity, and the best position it has previously attained. The particle with the highest fitness value is acknowledged as the global best position. As the swarm progresses, solutions are dynamically altered with a potential shift toward a region that holds promise for the global optimum. Notably, the speed at which a particle travels is dynamically adjusted based on the collective experiences of the swarm. Both personal best (pbest) and global best (gbest; gb) values are maintained for each particle. The alteration in a particle's position is contingent upon several factors: its current position, current velocity, the discrepancy between its present position and pbest (pb), and the variance between its current position and gbest. The velocity equation for the particles is given by Eq. (5), and the new position of the particles is derived using Eq. (6).

$$v_i^{t+1} = v_i^t + c_1 U_1^t \left(pb_i^t - p_i^t\right) + c_2 U_2^t \left(gb_i^t - p_i^t\right) \tag{5}$$

$$p_i^{t+1} = p_i^t + v_i^{t+1} \tag{6}$$

In the present research, the primary objective of employing the PSO algorithm lies in determining the optimal value of the condenser's geometric parameters. The algorithm's application aims to ascertain a combination of these parameters that bolsters the condenser's efficiency, keeping within pressure drop constraints in both the shell and tube, based on design data. Parameters chosen for optimization encompass tube length (Lt), tube outside diameter (tube OD), baffle spacing (B), shell diameter (Ds), number of tube passes (Np), and tube wall thickness (tw). These parameters were deemed crucial due to their independence from other geometric variables and their conformance to standard value ranges. Apart from enhancing the effectiveness value, solutions derived from the PSO algorithm are constrained to neither surpass nor diminish the design pressure drop values in the shell (ΔPs) and tube (ΔPt).

The objective function employed in the optimization procedure is tailored according to the maximum and minimum parameters under consideration. This study's goal centers on optimizing the highest effectiveness within the bounds of ΔPs and ΔPt. The operational domain of the objective function is delineated in Eqs. (7) and (8).

$$\Delta Ps = f_s \frac{G_s^2 \left(N_b + 1\right) D_s}{2\rho_s D_e} \tag{7}$$

$$\Delta Pt = \left(\frac{4 f_{rt} L_{ta} N_p}{\text{tube ID}} + N_p\right) \tag{8}$$

For a more comprehensive understanding, future studies might consider juxtaposing the PSO algorithm's efficiency in this context with other optimization algorithms, examining potential variations in effectiveness across different condenser configurations.

4 Result and Discussion

In an analysis of Figure 1, all involved parameters were utilized to formulate a data set. The temperatures at all inlets and outlets were recorded, facilitating the calculation of $\bar{h}$ using Eq. (1), and subsequently N_u through the parameters h, k, and D. Subsequent to these calculations, these temperatures were utilized to determine the film temperature, enabling the assessment of Re and Pr. At this juncture, values for N_u, Re, and Pr, in relation to the film temperature, were successfully discerned.

4.1 Grouping Dimensionless Numbers Based on Buckingham Pi Theorem

The procedure creates a formula containing dimensionless parameters from dimensional parameters which are involved in heat transfer system. The dimensionless formula represents a heat transfer process regardless of

the geometry of the system. In heat transfer process there are seven dimensional parameters involved including h, k, Cp, ρ, μ, v, and D. The number of dimensional parameters is denoted by s. Next step is to select a set of fundamental/primary dimensions which is in this case are M, L, T, and θ. The number of primary dimensions is denoted by q. The repeating parameters used in the formula equals to q thus there are four which are D, ρ, μ, and k. Then the number of dimensionless groups can be obtained from subtraction of q from $s(s-q)$. The equations of dimensionless groups which is constructed from repeating parameters can be developed as shown in Eqs. (9)-(11).

$$\pi_1 = D^a \rho^b \mu^c k^d v \tag{9}$$

$$\pi_2 = D^a \rho^b \mu^c k^d C_p \tag{10}$$

$$\pi_3 = D^a \rho^b \mu^c k^d h \tag{11}$$

Solving all equations together, obtain a=1, b=1, c=-1 and d=0. Substitute the values of a, b, c, and d into the dimension equation above and summarize to Re, Pr, N_u. After the seven forced convection parameters have been grouped into three dimensionless numbers, it is necessary to check whether the three numbers are truly dimensionless by using Eqs. (12)-(14).

$$\Pi 1 = \frac{D \cdot \rho \cdot v}{\mu} = \frac{\left[\mathrm{L} \cdot \frac{M}{L^3} \cdot \frac{L}{T}\right]}{\left[\frac{M \cdot L}{T}\right]} \tag{12}$$

$$\Pi 2 = \frac{\mu \cdot Cp}{k} = \frac{\left[\frac{M}{L.T} \cdot \frac{L^2}{T^{2\theta}}\right]}{\left[\frac{M \cdot L}{T^3 \theta}\right]} \tag{13}$$

$$\Pi 3 = \frac{D \cdot h}{k} = \frac{\left[\mathrm{L} \cdot \frac{M}{T^3 \theta}\right]}{\left[\frac{M \cdot L}{T^3 \theta}\right]} \tag{14}$$

All the three equations give dimensionless parameters in terms of N_u= $f(Re, Pr)$. The function of the impendence parameters further is determined using mathematical procedure by defining N_u as dependent variables and Re and Pr as the independent parameters as explained in part 2.2, Therefore, the heat transfer correlation can be inferred as Eq. (15).

$$N_u = C \cdot Re^m \cdot Pr^n = C \cdot \left(\frac{\mathrm{De} \cdot \rho \cdot \mathrm{v}}{\mu}\right)^m \cdot \left(\frac{\mu \cdot \mathrm{Cp}}{\mathrm{k}}\right)^n = \frac{\bar{h} \cdot \mathrm{De}}{\mathrm{k}} \tag{15}$$

4.2 Mathematical Procedures Employed

To scrutinize Eq. (15), mathematical methodologies such as Logarithmic Linear Regression Analysis, Power Law, and Curve Fitting were employed. Through these, the formula characterizing heat transfer, in terms of Re, Pr, and N_u, was resolved, leading to the determination of the power constants (n and m) as well as the constant C. Using the mechanical properties extracted from the empirical data of a specific industrial case, as presented in Table 2, Re and Pr were computed. Figure 3 illustrates a graph depicting log (N_u) as a function of log (Re). For the discernment of the trend line within this logarithmic graph, curve fitting was applied.

An analysis of Figure 3 reveals a correlation coefficient of 0.893 (m = 0.893) between the independent variable Re and the dependent variable N_u. This suggests a proportional relationship between Re and N_u, albeit with the increase in Re not significantly amplifying the heat transfer process (exponential/power to 0.893). An upsurge in Re might potentially be attributed to escalated water velocities or temperature variations on both fronts.

A secondary data set was formulated through manipulation of Eq. (4), whereby the parameter of log (N_u) divided by log (Pr) was represented as a function of the corresponding Re. This relationship is visually depicted in Figure 4. From the same figure, the power of n was determined to be 13.442, with C established at 1.15. Substituting the values of C, m, and n into Eq. (4), the equation was reframed as:

In a physical context, Re exemplifies the ratio of inertial to viscous forces, while Pr represents the ratio between momentum and thermal diffusivity. The heightened power coefficient of Pr underscores the pronounced influence of thermal phenomena over kinetic processes within the context of shell and tube heat exchangers. Such an observation aligns with the prevailing understanding that temperature plays a paramount role in the dynamics of heat exchanger systems.

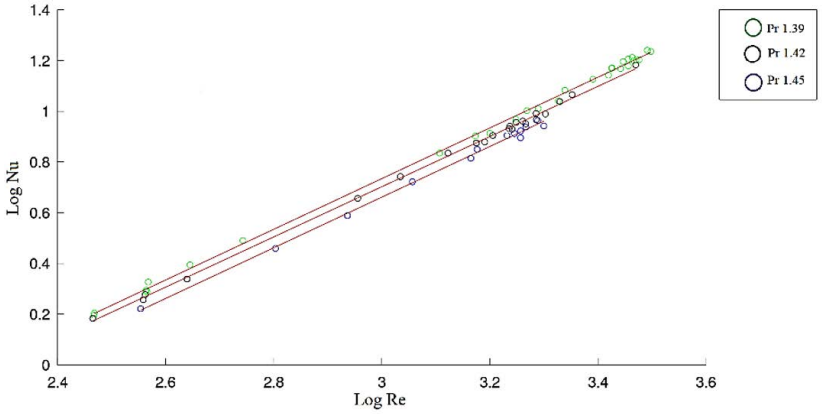

Figure 3. Representation of log (N_u) in relationship to log (Re)

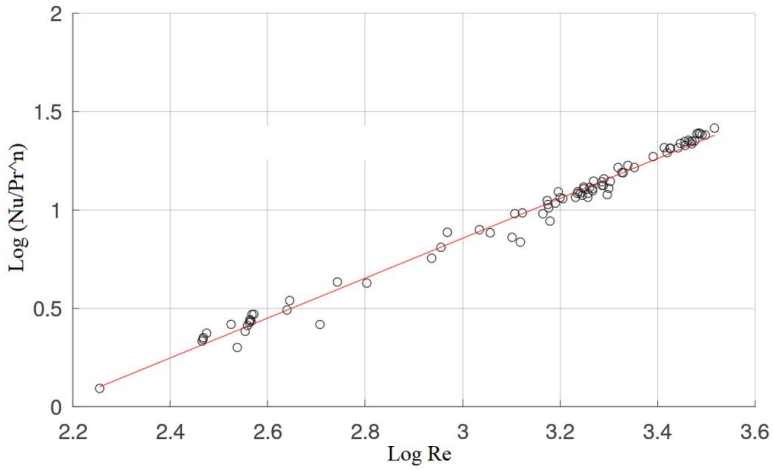

Figure 4. Curve fitting encompassing Reynolds, Prandtl, and the observed Nusselt number

4.3 Optimization Employing the PSO Algorithm

Leveraging the Tubular Exchanger Manufacturer Association (TEMA) standard, the independent geometric parameters identified to influence the condenser shell and tube's effectiveness and pressure drop values include tube length (Lt), tube outside diameter (tube OD), baffle spacing (B), shell diameter (shell ID), number of tube passes (np), and tube wall thickness (tw). For the determination of the objective function, effectiveness (ε) and pressure drop in the shell (ΔPs) and tube (ΔPs) were utilized. The optimization procedure aimed to enhance the ε value within the confines of ΔPs and ΔPt values given the operational data. The functional relationship of ε is presented in Eq. (16):

$$\varepsilon = f(Lt, tubeOD, B, Ds, np, tw) = \frac{q}{q_{\max}} \tag{16}$$

The relationship between the objective function and the governing parameters is depicted in Figure 5.
Max fobj (Lt, tube OD, B, Ds, np, tw) $\rightarrow$ function ε
Min fobj (Lt, tube OD, B, Ds, np, tw) $\rightarrow$ Δ Ps function
Min fobj (Lt, tube OD, B, Ds, np, tw) $\rightarrow$ ΔPt function

Table 3. Optimization result

Parameters	Optimization	
	Before	After
ε	0.9473	4.299
ΔPs	3216.5737	3216.4
ΔPt	2911.0031	2753.2

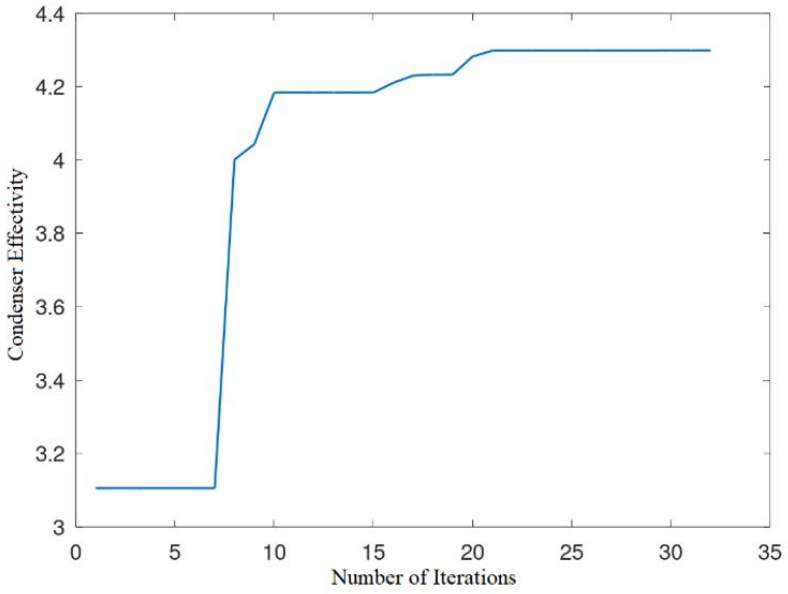

Figure 5. PSO algorithm optimization iteration graph

The execution of the PSO algorithm in the Octave software for optimizing the condenser's effectiveness produced the iteration graph represented in Figure 5. It was observed from Figure 5 that convergence was achieved on the 33rd iteration. The objective function's value, which is presented on the y-axis as ε, showed an increase from iterations 0 to 30, stabilizing between iterations 31 to 33.

Table 3 captures the changes in ε, ΔPs and ΔPt as a consequence of the optimization. An optimal $\mathcal{E}$ value of 4.299 was determined. To reach these results, the PSO algorithm rendered values for Lt, tube OD, B, Ds, np, and tw as 4.5159 m, 0.010267 m, 1.2814 m, 2.5238 m, 2 pieces, and 0.0004572m, respectively. Comparisons with the design data reveal reductions in the values of Lt by 30.5246%, tube OD by 46.1049%, B by 80.2861%, Ds by 7.9979%, np by 50%, and tw by 61.9%.

The enhancement in ε was attributed to the reduction in B size. A decrease in B size was correlated with increased steam turbulence within the shell. The number of baffles (nb) influences the heat transfer process duration. A rise in nb was found to extend the heat transfer time, thereby elevating effectiveness [27]. This, in turn, amplified the Reynolds number (Re) of the steam, resulting in increased convective coefficients and ε values.

From Table 3, a decrease in ΔPs by 0.0054% relative to the design data was observed. This reduction was anticipated, with the stipulation that ΔPs remains below the design threshold post-optimization. The decline in ΔPs was attributed to the B size exceeding the TEMA standard's minimum B value. An expanded B size culminated in fewer baffles (nb), diminishing steam flow collision within the shell against the baffles. This subsequently reduced steam flow turbulence, leading to a decline in ΔPs [22].

The ΔPt value underwent a 5.4209% reduction from the design data, aligning with expectations. The decline in ΔPt was linked to the reductions in Lt and tw values. Shorter fluid pathways, combined with a diminished tube wall thickness, were inferred to limit frictional forces between cooling water and the tube wall [4, 23]. This frictional force reduction, coupled with a decrease in np, was posited to result in a lower ΔPt value.

Alongside the changes in the aforementioned objective function values, six condenser geometric parameters—namely Lt, tube OD, B, Ds, np, and tw—also underwent modifications. These shifts instigated alterations in other parameters due to interdependencies among the geometric data. As a result, the condenser maintained adherence to existing design standards. Variations in other parameters, influenced by changes in the six optimization parameters, are presented in Table 4.

Upon optimization, it was observed that alterations in the parameters Lt, tube OD, B, Ds, np, and tw concurrently induced changes in other geometric parameters. Specifically, variations were noted in the tube inner diameter (tube ID), clearance between the tube bundle and shell (Lbb), the outer diameter limit (Dotl), the outer dimension of the tube bank (Dctl), the number of tubes (nt), the equivalent diameter (De), the number of baffles (nb), the clearance between tubes within the tube bundle (C'), the tube pitch (PT), and the flow area traversing the tube bundle (as). These observed modifications align with the TEMA standard, with the adjustments in Lt, tube OD, B, Ds, np, and tw remaining within the stipulated ranges: 3.048 m – 6.096 m for Lt; 0.0064 m – 0.0508 m for tube OD; 1.09728 m – 1.3716 m for B; 2.057 m – 2.54 m for Ds; 2 to 8 pieces for np; and 0.0004572 m – 0.004572 m for tw.

Table 4. Changes in condenser design data with optimization result data

Parameters	Design Data	Optimization	Discrepancy (%)
$\mathrm{Lt(m)}$	6.5	4.5159	30.5246
Tube OD (m)	0.01905	0.010267	46.1050
Tw (m)	0.0012	0.0005	61.9
Tube ID (m)	0.01785	0.0098	45.0431
$\mathrm{Lbb(m)}$	0.012	0.012	0.1143
$\mathrm{Dotl(m)}$	2.7312	2.5118	8.0336
$\mathrm{Dctl(m)}$	2.7121	2.5015	7.7662
nt (unit)	10634.2799	31145.2073	192.8756
np (unit)	4	2	50
Ds (m)	2.7432	2.5238	7.998
De $\mathrm{(m)}$	0.0281	0.0151	46.1050
nb (unit)	0	2.5242	0
$\mathrm{B(m)}$	6.5	1.2814	80.2862
$\mathrm{C'(m)}$	0.00476	0.0026	46.1050
$\mathrm{PT(m)}$	0.02381	0.0128	46.1050
As $\left(\mathrm{m^2}\right)$	3.56616	0.6468	81.8629
A $\left(\mathrm{m^2}\right)$	4134.7197	4534.2844	9.6648
hi $\left(\mathrm{m^2 \cdot K}\right)$	6751.70592	4821.7372	28.5855
ho $\left(\mathrm{m^2 \cdot K}\right)$	72.323	354.8961	390.7071
UD $\left(\mathrm{m^2 \cdot K}\right)$	69.2034	286.3815	313.8255

5 Conclusion

In the presented research, empirical and theoretical methodologies were developed to elucidate the forced convection heat transfer characteristics within the condensing region of the shell and tube heat exchanger. Employing the Buckingham Pi Theorem, three dimensionless parameters pertinent to heat transfer were derived. Subsequent application of Logarithmic Regression Analysis, Power Law Analysis, and Curve fitting Analysis facilitated the identification of power constants. As a result, the following relationship was established:

$$N_u = 1.15 \cdot Re^{0.893} \cdot Pr^{13.442}$$

Furthermore, optimization of the effectiveness within a specific pressure drop range in both the shell and tubes was achieved through the implementation of the PSO method. Following this optimization, a marked increase in effectiveness was observed, registering a value of 4.299, a significant ascent from the initial 0.9473.

The findings underscore the potential of integrating theoretical and empirical approaches in understanding and enhancing the performance of heat exchangers. Future investigations might delve deeper into the broader implications of these methodologies, particularly in varied operational conditions.

Data Availability

The data used to support the findings of this study are available from the corresponding author upon request.

Conflicts of Interest

The authors declare no conflict of interest.

References

[1] D. L. Gee and R. L. Webb, "Forced convection heat transfer in helically rib-roughened tubes," *Int. J. Heat Mass Transfer*, vol. 23, no. 8, pp. 1127–1136, 1980. https://doi.org/10.1016/0017-9310(80)90177-5

[2] A. P. Colburn, "A method of correlating forced convection heat-transfer data and a comparison with fluid friction," *Int. J. Heat Mass Transfer*, vol. 7, no. 12, pp. 1359–1384, 1964. https://doi.org/10.1016/0017-9310(64)90125-5

[3] A. M. Hussein, K. V. Sharma, R. A. Bakar, and K. Kadirgama, "A review of forced convection heat transfer enhancement and hydrodynamic characteristics of a nanofluid," *Renew. Sustain. Energy Rev.*, vol. 29, pp. 734–743, 2014. https://doi.org/10.1016/j.rser.2013.08.014

[4] K. Silaipillayarputhur and H. Khurshid, "The design of shell and tube heat exchangers–A review," *Int. J. Mech. Prod. Eng. Res. Dev.*, vol. 9, no. 1, pp. 87–102, 2019. https://doi.org/10.24247/ijmperdfeb201910

[5] Q. Li, K. H. Luo, Q. J. Kang, Y. L. He, Q. Chen, and Q. Liu, "Lattice Boltzmann methods for multiphase flow and phase-change heat transfer," *Prog. Energy Combust. Sci.*, vol. 52, pp. 62–105, 2016. https://doi.org/10.1016/j.pecs.2015.10.001

[6] D. Lakehal, "The role of computational multiphase flow modelling in flow assurance and gas processing," in *Proceedings of the 3rd International Gas Processing Symposium: Qatar*. Elsevier, 2012.

[7] G. Tryggvason, B. Bunner, A. Esmaeeli, and N. Al-Rawahi, "Computations of multiphase flows," *Adv. Appl. Mech.*, vol. 39, no. C, pp. 81–120, 2003. https://doi.org/10.1016/S0065-2156(02)39002-1

[8] M. Sommerfeld, "Numerical methods for dispersed multiphase flows," in *Particles in Flows*, 2017, pp. 327–396.

[9] Y. Shi, H. Zhu, J. Zhang, J. Zhang, and J. Zhao, "Experiment and numerical study of a new generation three-stage multiphase pump," *J. Pet. Sci. Eng.*, vol. 169, pp. 471–484, 2018. https://doi.org/10.1016/j.petrol.2018.06.011

[10] V. B. Nguyen, Q. B. Nguyen, Z. G. Liu, S. Wan, C. Y. H. Lim, and Y. W. Zhang, "A combined numerical–experimental study on the effect of surface evolution on the water–sand multiphase flow characteristics and the material erosion behavior," *Wear*, vol. 319, no. 1-2, pp. 96–109, 2014. https://doi.org/10.1016/j.wear.2014.07.017

[11] S. K. Gupta, H. Verma, and N. Yadav, "A review on recent development of nanofluid utilization in shell & tube heat exchanger for saving of energy," *Mater. Today Proc.*, vol. 54, pp. 579–589, 2022. https://doi.org/10.1016/j.matpr.2021.09.455

[12] Q. Wang, G. Chen, Q. Chen, and M. Zeng, "Review of improvements on shell-and-tube heat exchangers with helical baffles," *Heat Transf. Eng.*, vol. 31, no. 10, pp. 836–853, 2010. https://doi.org/10.1080/01457630903547602

[13] S. K. Gupta, S. Gupta, and R. Singh, "A comprehensive review of energy saving in shell & tube heat exchanger by utilization of nanofluids," *Mater. Today Proc.*, vol. 50, pp. 1818–1826, 2022. https://doi.org/10.1016/j.matpr.2021.09.212

[14] A. Costa and E. Queiroz, "Design optimization of shell-and-tube heat exchangers," *Appl. Therm. Eng.*, vol. 28, no. 14-15, pp. 1798–1805, 2008.

[15] V. K. Patel and R. V. Rao, "Design optimization of shell-and-tube heat exchanger using particle swarm optimization technique," *Appl. Therm. Eng.*, vol. 30, no. 11-12, pp. 1417–1425, 2010. https://doi.org/10.1016/j.applthermaleng.2010.03.001

[16] S. Fettaka, J. Thibault, and Y. Gupta, "Design of shell-and-tube heat exchangers using multiobjective optimization," *Int. J. Heat Mass Transf.*, vol. 60, pp. 343–354, 2013. https://doi.org/10.1016/j.ijheatmasstransfer.2012.12.047

[17] A. A. A. Arani and R. Moradi, "Shell and tube heat exchanger optimization using new baffle and tube configuration," *Appl. Therm. Eng.*, vol. 157, p. 113736, 2019. https://doi.org/10.1016/j.applthermaleng.2019.113736

[18] S. T. Sucahyo, "Annalis laju perpindahan panas dan efectivitas condenser unit 3 pltu pt. pjb up gresik annalis laju perpindahan panas dan efektivitas condenser unit 3 pltu pt." https://repository.its.ac.id/72369/1/2112030021-Non-Degree.pdf

[19] W. S. Robert, *Process Heat Transfer: Principles and Applications*. Texas, USA: Elsevier Science, 2007.

[20] P. J. Pritchard, *Fox and McDonald's Introduction to Fluid Mechanics*. USA: John Wiley & Sons, 2011.

[21] M. Gunes, "Computer aided heat transfer analysis in a laboratory scaled heat exchanger unit," *J. Chem. Inf. Model.*, vol. 53, no. 9, pp. 1689–1699, 2013.

[22] T. S. Park, "Computation of nusselt numbers on a tube with thin circular isothermal fins in laminar cross flow," in *IEEE Conference on Vehicle Power and Propulsion (VPPC)*. Seoul, Korea: IEEE, 2012, pp. 1059–1062. https://doi.org/10.1109/VPPC.2012.6422501

[23] G. S. Gupta, S. Sarkar, A. Chychko, L. D. Teng, M. Nzotta, and S. Seetharaman, "Chapter 3.1-Process concept for scaling-up and plant studies," in *Treatise on Process Metallurgy*, pp. 1100–1144. https://doi.org/10.1016/B978-0-08-096988-6.00040-7

[24] R. Muwanga and I. Hassan, "Local heat transfer measurements in microchannels using liquid crystal thermography: Methodology development and validation," *J. Heat Transf.*, vol. 128, no. 7, pp. 617–626, 2006. https://doi.org/10.1115/1.2193541

[25] N. Zheng, P. Liu, F. Shan, Z. Liu, and W. Liu, "Effects of rib arrangements on the flow pattern and heat transfer in an internally ribbed heat exchanger tube," *Int. J. Therm. Sci.*, vol. 101, pp. 93–105, 2016. https://doi.org/10.1016/j.ijthermalsci.2015.10.035

[26] N. Koçyigit and H. Bulgurcu, "Modeling of overall heat transfer coefficient of a concentric double pipe heat exchanger with limited experimental data by using curve fitting and artificial neural network combination," *Therm. Sci.*, vol. 23, no. 6, pp. 3579–3590, 2018. https://doi.org/10.2298/TSCI171206111K

[27] B. Melissari and S. A. Argyropoulos, "Development of a heat transfer dimensionless correlation for spheres immersed in a wide range of prandtl number fluids," *Int. J. Heat Mass Transf.*, vol. 48, no. 21-22, pp. 4333–4341, 2005. https://doi.org/10.1016/j.ijheatmasstransfer.2005.05.025